SolarPACES 2024, 30th International Conference on Concentrating Solar Power, Thermal, and Chemical Energy Systems

Solar Fuels and Chemical Commodities

https://doi.org/10.52825/solarpaces.v3i.2438

© Authors. This work is licensed under a Creative Commons Attribution 4.0 International License

Published: 18 Nov. 2025

# Solar-Driven Biomass Pyrolysis Plant for Negative-Emission Biofuels Production

Muhammad Ahsan Amjed<sup>1</sup>, Marco Colombi<sup>1,\*</sup>, Juan Pablo Rincon Duarte<sup>2</sup>, Clarisse Lorreyte<sup>2</sup>, Gkiokchan Moumin<sup>2</sup>, Matteo Carmelo Romano<sup>1</sup>, and Marco Binotti<sup>1</sup>

<sup>1</sup>Department of Energy, Politecnico di Milano, Italy <sup>2</sup>German Aerospace Center (DLR), Germany

\*Correspondence: Marco Colombi, marco.colombi@polimi.it

Abstract. As part of the Horizon Europe Project PYSOLO, this study focuses on the integration of a 10 MW<sub>TH</sub> fast pyrolysis plant with a solar tower system equipped with a rotary kiln particle receiver. Heated particles act as a particle heat carrier (PHC) for the endothermic pyrolysis process, enhancing flexibility and allowing continuous operation compared to directly heated solar reactors. The system's design, techno-economic analysis and storage capacity optimization are performed considering two operation modes, solar-only and hybrid, in which biochar is combusted in absence of solar energy. Results indicate that, due to the rotary kiln flow regime constraints, its tilt angle has to be limited in a range between 0.5-2° to guarantee particles being in rolling mode, thus penalizing the achievable solar field optical efficiency. On the other hand solar-based pyrolysis can achieve carbon efficiencies close to 0.9 and, thanks to the carbon stored in biochar, net negative emissions equal to -27.05 and -19.45 kg<sub>CO2</sub>/GJ<sub>OIL</sub> respectively in solar-only and hybrid mode. Moreover, as the pyrolysis section has the most relevant cost share, the system optimization pushes to maximise the pyrolysis plant operating hours (and thus the bio-oil production) to reduce the CAPEX impact on the Minimum Fuel Selling Price (MFSP). For this reason hybrid mode results in being the most convenient (i.e: MFSP of 25.71 vs 21.36 €/GJ<sub>OIL</sub>).

Keywords: Biomass; Solar Pyrolysis; Concentrated Solar Power; Bio-Oil; Biochar

#### 1. Introduction

According to the European Union (EU) the fraction of renewables in the EU energy mix is expected to grow up to at least 42.5% by 2030 [1], an ambitious threshold that has driven research and industry efforts in developing new ways of exploiting renewable energy sources. Nowadays bioenergy provides 12.6% of the overall energy consumption [2] and can be converted into higher density energy vectors either by a thermochemical or biochemical process. Thermochemical conversion benefits from faster chemical reactions, suitability for a wider variety of biomass feedstock, higher energy efficiency and advantages of scalability compared to biochemical processes. Moreover, thermochemical conversion is not subject to seasonal and environmental limitations as biochemical and allows year-long operation with better control of operating conditions [3]. Based on the amount of supplied oxygen, a thermochemical process can be classified as pyrolysis, combustion or gasification. Pyrolysis in particular has gathered great interest due to its potential of converting any type of solid biomass into bio-oil, whose most promising application is co-processing in Fluid Catalytic Crackers (FCC) in existing fossil

refineries [4], and/or biochar, a way to concentrate stable carbon in large amounts and use it in agriculture as soil amendment, as heat, as material in a variety of applications or as a carbon sequestration medium [5]. The pyrolysis process is endothermic and requires an external energy source, such as direct combustion of part of the feedstock/products or electric heating, to heat up the feedstock and break down the molecular structure of the carbonaceous material [6]-[9]. The limit of conventional pyrolysis processes sustained by combustion is the loss of part of the biogenic carbon as CO<sub>2</sub>, increasing the environmental impact and losing a valuable asset, thus making the process more energy intensive and costly. In the literature, the adoption of Concentrated Solar Power (CSP) as energy source to overcome those limits has been gaining attention, considering different feedstocks, types of concentrators, reactors and process configurations [6]-[9].

As part of the Horizon Europe Project PYSOLO [10], this analysis focuses on the integration of the pyrolysis unit with a solar tower system equipped with a rotary kiln particle receiver: the particles heated in the tower are directly used as heat carrier (particle heat carrier, PHC) in the pyrolyzer to provide the required thermal power for the endothermic pyrolysis process. Compared to directly irradiated biomass reactors, the decoupling between solar receiver and pyrolizer enhances flexibility and allows continuous operation with possible thermal energy storage integration. On the other hand, the adoption of a particle receiver in place of a commercial molten salts solar tower is meant to avoid the molten salts high corrosiveness, the high solidification temperature that makes start-up and shut-down problematic causing high parasitic losses, and the need of a high temperature heat transfer surface thanks to the direct contact between PHC and biomass.

In the following study, the preliminary design and the techno-economic analysis of a 10 MW<sub>TH</sub> fast pyrolysis plant for bio-oil and biochar production integrated with a rotary kiln particle solar tower system are performed comparing different plant configurations (solar-only and hybrid). For each plant configuration, the storage capacity and the solar multiple (SM) are optimized in order to minimize the minimum fuel selling price (MFSP), which is obtained following a net present value (NPV) analysis. Being biomass made of biogenic carbon and thus being carbon neutral, focus is given to the potential negative  $CO_2$  emissions of both plant configurations, which, by storing or using as soil amendment the biochar produced, can act as a carbon sequestrator plant.

# 2. System Modelling

This section introduces the main modelling assumptions of the pyrolysis plant, of the rotary kiln solar receiver and of the economic and profitability analysis.

### 2.1 Pyrolysis Plant

The configuration of the fast pyrolysis section is taken from Jones et al. [7], where a biorefinery converting woody biomass into high-value liquid fuel was modelled. In a previous study [11], the model has been replicated and slightly modified to account for the solar integration adopting Aspen Plus V14 [12] to compute mass and energy balances. The plant is sized to convert a biomass input of 50 dry t/d (10 MW $_{\text{TH}}$  on a lower heating value basis) and is divided into 5 main sections as shown in Figure 1:

- Biomass Pretreatment: for an efficient conversion, biomass is dried till reaching a moisture content of 10% by a stream of hot flue gases and is then grinded to 2 mm particles to ease the pyrolysis reaction. The biomass properties are summarized in Table 1.
- Pyrolysis: dried biomass enters the pyrolyzer and is converted by contact with hot PHC and fluidizing gases. The temperature of the hot PHC is 609°C and the flowrate is con-

trolled to maintain the reactor outlet temperature equal to 434°C. The fluidized bed pyrolyzer is modeled as a black box with fixed biomass input, replicating the yield and product composition reported by Jones et al. [7] and considering the PHC as chemically inert.

Elemental Analysis (%wt on dry basis)	Proxi- mate Analysis (%wt on dry basis)	Calorific Values	Elemental Analysis (%wt on dry basis)	Proximate Analysis (%wt on dry basis)	Calorific Values	
С	50.94	Volatile Matters	84.88	HHV [MJ/kg]	14	
Н	6.04	Voiatile Matters				
0	41.90	Fixed Carbon	14.2		10.0	
N	0.17	Fixed Carbon	14.2	LHV [MJ/kg]	12.3	
S	0.03	Ashes	0.02	Humidity (dry basis)		
Ashes	0.92	Asnes	0.92	30%		

Table 1. Properties of the adopted biomass (Poplar).

- Solid Removal: the products enter the cyclone filter, which is responsible for the separation
  of volatile products from solids entrained from the reactor at high temperatures.
- Bio-Oil Recovery: quenching columns are used for the condensation of pyrolysis vapours and collection of bio-oil. The non-condensable gases generate the so-called pyrogas, mainly composed by CO, CO<sub>2</sub> and CH<sub>4</sub>, whose majority is used as a fluidizing medium while the remaining fraction is combusted to generate heat for the drying process. Bio-oil is then filtered to remove solid particles along with a small portion of oil, generating the so-called sludge.
- Solid Separator: the PHC is separated from the biochar and is sent to the cold solid Thermal Energy Storage (TES) after a make-up to compensate for PHC losses.

Two different plant configurations are analysed, solar-only and hybrid. In solar-only mode the pyrolysis plant works only when solar energy is available while in hybrid mode the plant always works, compensating the absence of solar energy by burning the sludge and a fraction of the produced biochar in a combustor, heating up the PHC.

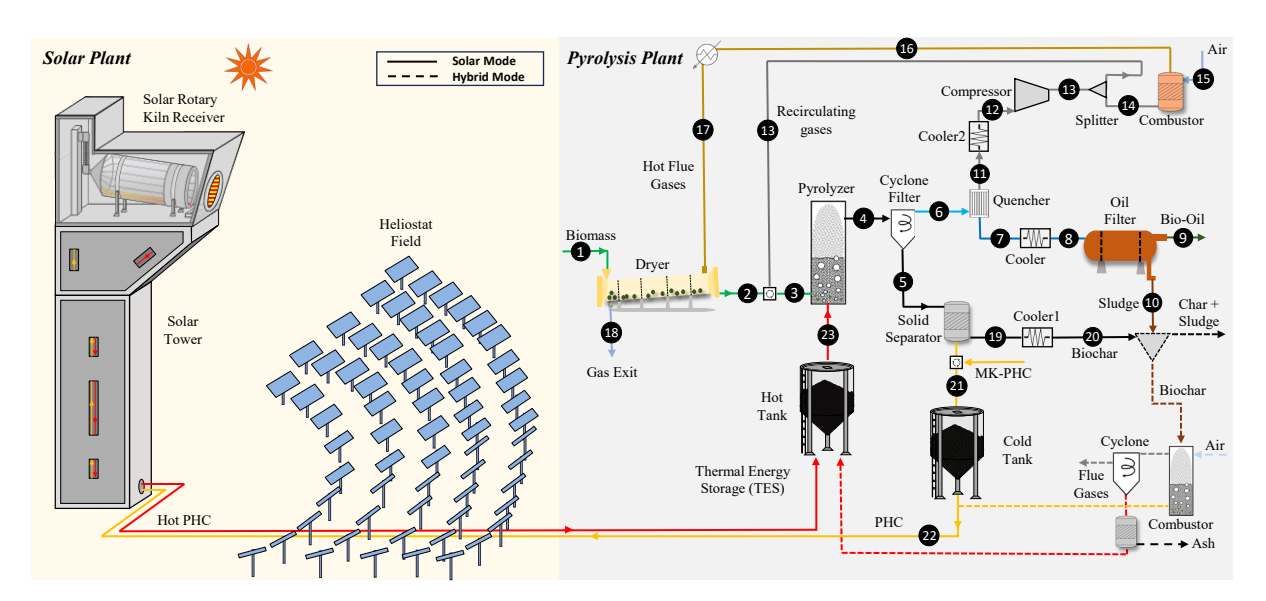


Figure 1. Assessed system scheme. Dashed lines represent hybrid system operation.

To compare the performances of the two configurations, a series of key performance indicators (KPIs) can be considered. The pyrolysis plant energy conversion efficiency  $\eta_{pyro-plant}$  is defined in Eq.(1) as the ratio between the products chemical energy (bio-oil, biochar, sludge)

and the primary energy input, where  $\dot{m}_{prod,i}$  and  $LHV_i$  are the mass flowrate and the lower heating value of the *i*-th product,  $\dot{m}_{biom}$  is the biomass flowrate,  $P_{AUX}$  is the plant overall electric consumption,  $\eta_{el,ref}$  is the reference thermal to electrical energy efficiency (assumed equal to 50%), and  $\dot{Q}_{PHC,nyre}$  is the thermal power provided via the PHC to the pyrolysis unit.

$$\eta_{pyro-plant} = \frac{\sum_{i} \dot{m}_{prod,i} \cdot LHV_{prod,i}}{\dot{m}_{biom} \cdot LHV_{biom} + \left(\frac{P_{Aux}}{\eta_{el,ref}}\right) + \dot{Q}_{PHC,pyro}} \tag{1}$$

The solar plant is defined by its solar optical-to-thermal efficiency  $\eta_{sol-th}$  which takes into account both solar field and receiver efficiency.

$$\eta_{sol-th} = \eta_{opt,SF} \cdot \eta_{th,kiln} = \frac{\dot{Q}_{rec}}{A_h \cdot DNI} \cdot \frac{\dot{Q}_{PHC,rec}}{\dot{Q}_{rec}}$$
(2)

The carbon efficiency  $\varepsilon_c$  is defined in Eq.(3), where  $y_{C,prod,i}$  and  $y_{C,biom}$  are the carbon mass fractions of the i-th product and of biomass, while the emission to oil ratio (ETO) and the net negative emission to oil ratio (ETO<sub>net</sub>) are defined in Eq.(4), where ETO is the ratio between pyrolysis plant yearly CO<sub>2</sub> emissions and bio-oil production while ETO<sub>net</sub> considers that biogenic CO<sub>2</sub> emissions are climate neutral, computing the negative emissions associated to having stored carbon inside biochar.

$$\varepsilon_C = \frac{\sum_i \dot{m}_{prod,i} \cdot y_{C,prod,i}}{\dot{m}_{biom} \cdot y_{C,biom}} \tag{3}$$

$$ETO = \frac{e_{CO2}}{Oil_t} \quad | \quad ETO_{net} = -\frac{\dot{m}_{char,i} \cdot y_{c,char} \cdot 44/_{12}}{Oil_t}$$
 (4)

The resulting bio-oil and biochar temperatures, flowrates and compositions together with the system overall carbon balance are reported in Table 2, while the main technical assumptions and preliminary design results considering Bauxite as PHC are reported in Table 3. In solar-only mode,  $\epsilon_c$  can be seen as the sum of bio-oil, biochar and sludge contributions to the carbon balance, while in hybrid mode  $\epsilon_c$  will depend on how much sludge and biochar will be burned throughout the yearly simulation.

**Table 2.** Bio-oil, biochar, sludge and flue gases flowrate, temperature, elemental composition and carbon balance.

Component	Flow [kg/h]	Tempera- ture [°C]	Composition [% mass]					% С	
Component			С	Н	0	N	Ashes	PHC	Yield
Bio-Oil (9)	1732	54.4	41.6	7.8	50.6	0.0	-	-	69.0
Biochar (20)	246	25	83.1	1.7	6.6	1.4	7.1	-	19.6
Sludge (10)	59	54.4	38.3	7.2	46.6	-	2.4	5.4	2.2
Flue gases (18)	4555	71.7	2.1	1.7	34.7	61.5	-	-	9.2

Table 3. Main technical assumptions and preliminary design results.

Parameter	Value	Parameter	Value
Biomass Flowrate (30% HR) [kg/h]	2930	Pyrolyzer Net Thermal Request [MW]	1.66
Pyrolyzer Outlet T [°C]	434	Pyrolyzer Heat Loss [MW]	0.1
PHC T Hot [°C]	609	Overall Electricity Consumption [kW]	353.2

#### 2.2 Solar Field and Receiver

Rotary kilns are widely employed for several industrial processes due to the uniform particles mixing, that ensures homogeneous temperatures at the outlet. The solarization of rotary kilns presents challenges related to: i) the effective penetration of the solar radiation inside the kiln to assure homogeneous temperature distribution, especially for significant length, ii) the limitation of the re-irradiation losses from the kiln aperture, iii) the cooling and the cleaning of the kiln window aperture and secondary mirror (if present) and iv) the selection of an optimal tilt angle considering the trade-off between solar field efficiency and process parameters (e.g. bed motion, particle mixing, residence, etc.) [13] [14].

The particles flow regime in the rotary kiln depends on the Froude number, defined in Eq. (5) as the ratio between centripetal and gravitational acceleration, where  $\omega_{kiln}$  and  $D_{kiln}$  are respectively the kiln rotational speed and its diameter. To correctly operate the rotary kiln maximizing the particles mixing, the Froude number has to range between  $10^{-4}$  and  $10^{-2}$  in order for the particles to be in rolling mode [15], where two distinct regions can be discerned: the shearing region, called the active layer, formed by particles near the free surface, and the passive or plug flow region at the bottom where the shear rate is zero [16] [17], as shown in Figure 2.

$$F_r = \frac{\omega_{kiln}^2 \cdot D_{kiln}}{2g} \tag{5}$$

Other relevant design parameters are:

• The Fill Ratio (FR), which is the fraction of the rotary kiln cross section occupied by the particles determining the particle bed center angle  $\delta_{bed}$  as shown in Figure 2. The FR can be determined also using Eq. (6), where  $\dot{m}_{PHC}$  is the design PHC flowrate given a certain Solar Multiple (SM),  $\tau_{res}$  is the kiln residence time,  $V_{kiln}$  is the kiln volume and  $\rho_{PHC}$  is the PHC bulk density. Typically FR ranges between 0.1-0.25 [13].

$$FR = \frac{\dot{m}_{PHC} \cdot \tau_{res}}{V_{kiln} \cdot \rho_{PHC}} \tag{6}$$

• The kiln residence time  $\tau_{res}$ , which depends on many factors like the kiln tilt angle  $\delta_{kiln}$ , the kiln angular speed  $\omega_{kiln}$  and the kiln aspect ratio  $L_{kiln}/D_{kiln}$ . The literature contains lots of empirical correlations [16] and in this study the simplified correlation from Lee and Lin [18] has been adopted, as shown in Eq. (7).

$$\tau_{res} = 0.19 \cdot \frac{L_{kiln}}{D_{kiln}} \cdot \frac{1}{\delta_{kiln} \cdot \omega_{kiln}} \tag{7}$$

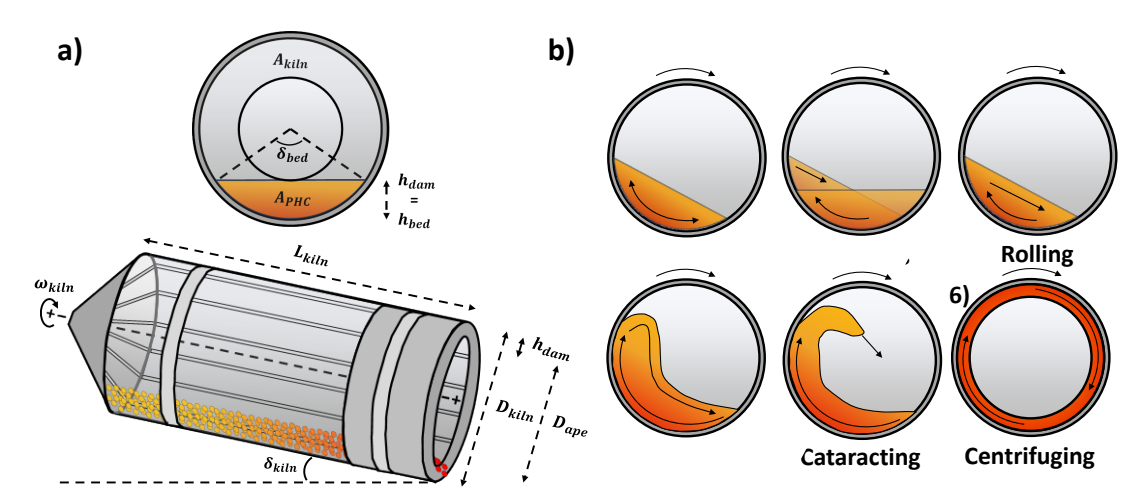


**Figure 2.** a) Geometric considerations of the rotary kiln design (adapted from [15]); b) Flow regimes in rotating drums with increasing Froude number (adapted from [16]).

• The dam height, which allows maintaining the particle bed inside the reactor with an almost constant height along the axial direction to favour particle mixing and to increase the residence time [13]. The dam height  $(h_{dam})$  has to be lower or close to the predicted bed height and in this study is considered equal to the bed height  $(h_{bed})$  [13], which can be found, together with the kiln aperture diameter  $D_{ape}$ , once the FR and the kiln diameter have been selected, as shown in Eq. (8).

$$h_{dam} = \frac{D_{kiln}}{2} \cdot \left\{ 1 - \cos \left[ \frac{\tilde{\delta}_{bed}(FR)}{2} \right] \right\} \mid D_{ape} = (D_{kiln} - 2h_{dam})$$
 (8)

In order to preliminarily design the rotary kiln assuring the correct Froude number range, equations (4) to (7) can be combined to explicit the rotary kiln diameter, which can be computed once the Froude number, the fill ratio FR, the kiln tilt angle  $\delta_{kiln}$ , the PHC bulk density  $\rho_{PHC}$  and the PHC flowrate  $\dot{m}_{PHC}$  have been imposed, as shown in Eq. (9). In this analysis, a fill ratio equal to 0.1 is chosen to increase the kiln diameter as much as possible to help achieve a decent solar field optical efficiency, as discussed later. The design Froude number is chosen so that its minimum boundary value is reached during the minimum solar plant partial load, equal to 20%. Being  $F_r \propto \omega^2$  and being  $\omega \propto \dot{m}_{PHC}$  at constant FR, the minimum Froude number boundary value is increased by a factor of 25, reaching  $2.5 \cdot 10^{-3}$ . The kiln diameter is thus obtained as:

$$D_{kiln} = \left(\frac{1.52 \, \dot{m}_{PHC}}{\rho_{PHC} \, \delta_{kiln} \, FR \, \sqrt{2 \, g \, F_r}}\right)^{2/5} \tag{9}$$

Once the kiln diameter is obtained, it is possible to compute the aperture size according to Eq. (7) and subsequently the thermal performance of the system, considering the following simplified energy balance, where the contribution of reflective, radiative and convective losses is considered:

$$\dot{Q}_{PHC} = \dot{Q}_{rec} - \dot{Q}_{refl} - \dot{Q}_{rad} - \dot{Q}_{conv} = \dot{Q}_{rec}\alpha - \sigma\varepsilon A_{ape} \left(T_{kiln}^4 - T_{amb}^4\right) + h_{cv}A_{ape} \left(T_{kiln} - T_{amb}\right) \tag{10}$$

where  $\alpha$  and  $\varepsilon$  are the effective solar absorptivity and emissivity,  $T_{kiln}$  is the average kiln cavity temperature, assumed for simplicity as the average temperature between the inlet and outlet PHC temperature, and  $h_{cv}$  is the convective heat transfer coefficient that considers both forced and natural convection contributions. The convective heat transfer coefficients are computed according to the following set of equations [13]:

$$h_{cv} = h_{n,cv} + h_{f,cv} \tag{11}$$

$$h_{f,cv} = \frac{k}{D_{kiln}} N u_{f,cv} = \frac{k}{D_{kiln}} 0.1967 \cdot v_{wind}^{1.849}$$
 (12)

$$h_{n,cv} = \frac{k}{D_{kiln}} N u_{n,cv} = \frac{k}{D_{kiln}} \left[ 0.088 \cdot Gr^{\frac{1}{3}} \cdot \left( \frac{T_{kiln}}{T_{amb}} \right)^{0.18} \cdot \left[ \cos(\delta_{kiln}) \right]^{2.47} \left( \frac{D_{ape}}{D_{kiln}} \right)^{S} \right]$$
(13)

$$S = 1.12 - 0.982 \left( \frac{D_{ape}}{D_{kiln}} \right) \tag{14}$$

$$Gr = \frac{\beta g (T_{kiln} - T_{amb}) D_{kiln}^3}{v^2} \tag{15}$$

where the air thermal conductivity k, the dynamic viscosity  $\nu$  and the volumetric expansion coefficient  $\beta$  are computed at  $T_{\infty} = T_{amb}$  as reported in [13]. The heat flux entering the kiln aperture can then be obtained with Eq. (16):

$$\phi_{rec} = \frac{\dot{Q}_{rec}}{A_{ape}} = \frac{\dot{Q}_{PHC} + \dot{Q}_{rad} + \dot{Q}_{conv}}{\alpha A_{ape}}$$
(16)

The rotary kiln energy balance and its size, determined by the flow regime constraints, are thus strongly bound. The kiln aperture diameter and the corresponding heat flux are reported in Figure 3 for different tilt angles and different Solar Multiples (SM, i.e.  $\dot{Q}_{PHC}/\dot{Q}_{pyro}$ ), considering bauxite as PHC. Results show how increasing the tilt angle, which is expected to be beneficial for the design of the solar field, reduces the allowed aperture size and increases the required heat flux to values that may be unfeasible. For the selected case the tilt angles need thus to be limited below 4-5° (i.e. fluxes below 2-3 MW/m²). To compensate for the aperture diameter reduction, an increase of rotational speed is needed to maintain constant the design Fr number.

For the solar field design, Seville (37.39° N, 5.99° W) is selected as plant site and a design DNI of 900 W/m² is assumed at solar noon on June 21th. The design is performed with SolarPILOT [19], considering a flat plate receiver geometry and a square aperture shape with a size equal to the kiln aperture diameter. As in SolarPILOT it is not possible to simulate a circular aperture, a correction coefficient of 0.94 to the obtained optical efficiency is applied: this value is an average value obtained by exporting the solar field from SolarPILOT to SolTrace [20] and then changing the receiver from square to circular.

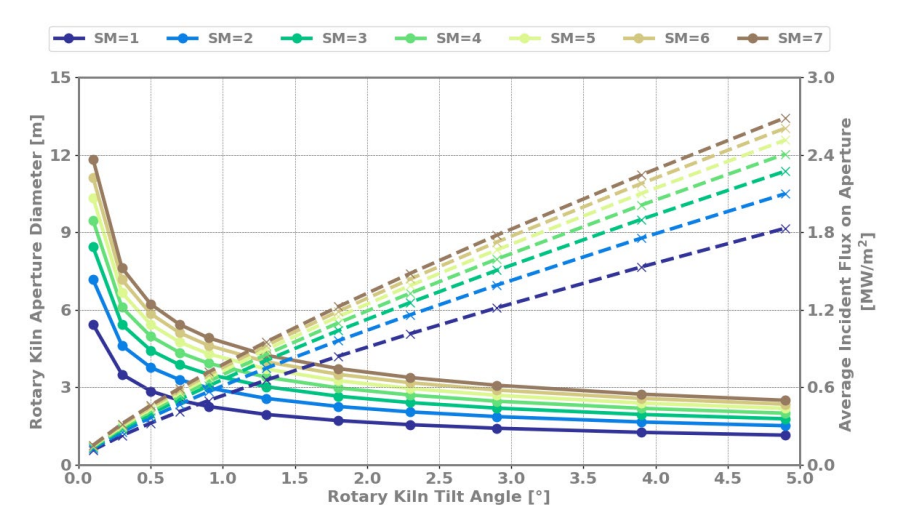


**Figure 3.** Kiln aperture diameter and corresponding heat flux at the receiver aperture for different tilt angles considering bauxite as PHC.

The tower height is varied between 60 and 120m in order to maximise the power absorbed by the PHC in design conditions. The consumption associated with the particle lift is also included in the auxiliaries calculation, according to Eq. (17). The other set of assumptions adopted for solar field design is reported in Table 4, consistently with [11], while the values of effective absorptivity and emissivity adopted for the rotary kiln simulation are taken from [13].

$$P_{lift} = \frac{\dot{m}_{PHC}gH_{tow}}{\eta_{lift}} \tag{17}$$

For every SM the best performing plant in terms of solar-to-thermal efficiency is selected and the optical efficiency for every combination of Azimuth and Zenith angles is computed with SolarPILOT: the obtained matrix is then used for the yearly analysis, performed with hourly resolution using DNI data from the SolarPILOT database. The off-design thermal performance of the rotary kiln is computed assuming constant temperatures and, as first approximation, constant radiative and convective losses, with reflective losses proportional to the incoming solar radiation.

Parameter	Value	Parameter	Value
Design DNI [W/m²]	900	PHC inlet/outlet temperature [°C]	434/609
Design Point	21 <sup>st</sup> June, Solar Noon	PHC Bulk Density [kg/m³]	2000
Heliostat size [m²]	16	PHC Mean Heat Capacity [J/kg K]	1124
Heliostat focusing type	At slant	PHC Mass flowrate, SM=1 [kg/s]	8.79
Heliostat error [mrad]	3.07	Design kiln Fr number [-]	2.5·10 <sup>-3</sup>
Heliostat reflectivity [-]	0.95	Design filling ratio [-]	0.1
Receiver acceptance angle [°]	75	Effective cavity emissivity [-]	0.9
Lift efficiency [-]	0.80	Effective cavity absorptivity [-]	0.95
Design power to the PHC, SM=1 [MW]	1.76	Wind speed at receiver height [m/s]	10

**Table 4.** Design assumptions for the receiver and solar field design.

### 2.3 Economic and Profitability Analysis

The economic and profitability analysis are carried out for an N<sup>th</sup>-of-a-kind plant, with assumptions and methodology consistent with NREL [7] and explained in detail in a previous study [11]. The method takes into account fixed and operational costs, requiring the calculation of the yearly discounted cash flows and aims at identifying the Minimum Fuel (bio-oil) Selling Price (MFSP) to have a NPV equal to zero at the end of the plant lifetime. The main economic assumptions are reported in *Table 5*. With respect to the previous study [11], the pyrolysis plant CAPEX has been slightly adjusted adding the bio-oil filter cost (~0.3 M€<sub>2019</sub> [7]), which was previously considered as part of the plant utilities CAPEX. The biomass cost has been updated while the rotary kiln receiver cost has been taken from the correlations developed by Buck et al. [21,22,23].

Parameter	Value	Parameter	Value
Computed CAPEX Pyrolysis Plant (Solar-only Mode) [M€]	20.07	Receiver Specific Cost [€/m²]	76300 [24]
Computed CAPEX Pyrolysis Plant (Hybrid Mode) [M€]	21.44	Tower Specific Cost [€/m <sup>1.9274</sup> ]	148.4 [21]
Biomass Cost [€/ton] [10% RH]	23.85 [25]	Thermal Energy Storage Specific Cost [€/m²]	1000 [22]
Electricity Cost [€/MWh <sub>EL</sub> ]	100	Bauxite Particles Cost [€/kg]	400 [26]
Heliostat Field Cost [€/m2]	133 [19]	Particle Elevator Cost [€ s/m kg]	53.55 [27]

**Table 5.** Main economic assumptions.

#### 3. Results

As explained in section 2.2, for every solar multiple the rotary kiln receiver tilt angle and the tower height have been optimized, while the kiln aperture diameter, considering the large mass flow rates and the given  $\Delta T$ , is determined by the constraints on the required flow regime. An example of the obtained solar-to-thermal efficiencies is reported on the left in Figure 4 for all the considered SM and tower heights.

Results are reported only for tilt angles equal to 0.5° and 0.9°, which represent the best performing cases. This is clearly shown on the right in Figure 4, where the main results for SM equal to 3 and for two tower heights (80m solid line and 100m dashed line) are reported: as the tilt angle grows, the constraint on the minimum Fr number requires a reduction of the kiln diameter and thus of the kiln aperture, which on one side guarantees higher thermal efficiencies but on the other reduces the solar field intercept factor and thus the optical efficiency. The compromise between these two opposite trends allows to identify the best solar-to-thermal efficiency.

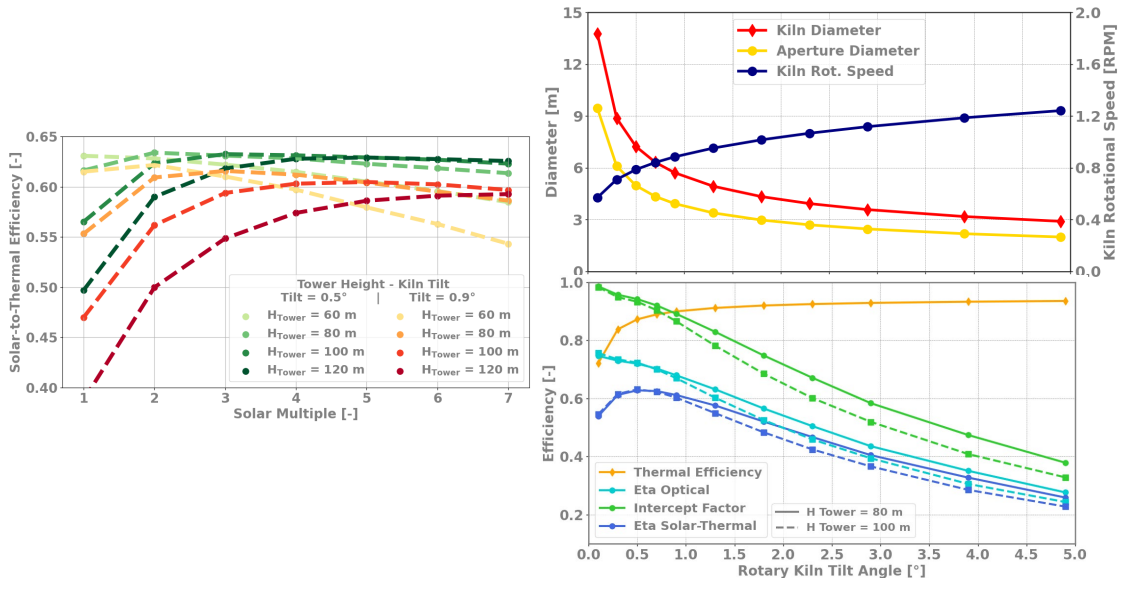


**Figure 4.** (Left) Optical-thermal efficiency for different SM and tower height for 2 different tilt angles. (Right) Trend of the solar filed efficiencies and size and rotational speed of the receiver for different kiln tilt angles and SM=3.

The main design results for the best performing solar plants in terms of solar-to-thermal efficiency for every SM are reported in Table 6. As it can be observed, increasing the SM the tower height increases in order to minimize cosine losses. On the other hand, since both kiln and aperture diameter are extremely sensible to variations in tilt angle due to the constraints on the required flow regime, the optimal range of tilt angles remains constant for each SM analysed in order to get a decent optical-thermal efficiency. To compensate for the reduction in kiln diameter increasing SM and maintain a constant Fr, the kiln rotational speed decreases. The optimized solar plants reported in Table 6 are then coupled with the pyrolysis plant and the storage size that minimizes the MFSP for each SM is identified, both for the solar-only and for the hybrid modes.

Table 6. Main design results for the optimized solar cases.

SM [-]	1	2	3	4	5	6
Q PHC [kW]	1760	3520	5280	7040	8800	10560
PHC Mass Flowrate [kg/s]	8.94	17.88	26.82	35.76	44.70	53.64
					Optimized	variables
Rotary Kiln Tilt $\delta_{kiln}$ [°]	0.7	0.5	0.5	0.5	0.5	0.5
Tower Height [m]	60	80	100	110	110	110
						Results
Kiln Diameter [m]	3.63	5.48	6.44	7.23	7.90	8.50
Aperture Diameter [m]	2.50	3.76	4.43	4.96	5.43	5.84
Kiln Rotational Speed [RPM]	1.11	0.90	0.83	0.79	0.75	0.72
Heliostat Area [m²]	3073	6083	9141	12199	15287	18391
Optical Efficiency [-]	0.724	0.735	0.728	0.724	0.719	0.715
Thermal losses [kW]	254	554	788	1012	1230	1444
Thermal efficiency [-]	0.873	0.862	0.868	0.872	0.876	0.878
Solar-to-thermal efficiency [-]	0.631	0.633	0.632	0.632	0.630	0.628

The yearly results and the economic performance of the best performing cases are reported in Table 7. The optimal SM for solar-only and hybrid mode is equal to 6 and 3 respectively and the CAPEX breakdown is reported in Table 7. The pyrolysis plant has a higher cost in hybrid mode due to the presence of the solid combustor and it constitutes roughly 78% of the total CAPEX, while the receiver cost constitutes roughly 17% of the solar plant CAPEX. As the pyrolysis section has the most relevant cost share, the system optimization pushes to maximise the pyrolysis plant operating hours (and thus the bio-oil production) to reduce the CAPEX impact on the MFSP. In the optimization of the plant operating in solar-only mode, the maximum storage size was limited to 24h and the pyrolysis plant is not able to achieve full equivalent hours of operation during the year, thus affecting the Minimum Fuel Selling Price (MFSP), which is higher with respect to the one in hybrid mode, equal to 21.36  $\epsilon$ /GJ<sub>OIL</sub>. On the other hand the carbon efficiency, the ETO and the ETO<sub>NET</sub> are in favour of the solar only mode since no combustion is allowed. In any case both plants reach negative emissions, thus being suitable as carbon sequestrators in the future.

**Table 7.** Main results of the optimized Solar-Only and Hybrid cases.

Results	Solar-Only	Hybrid
Optimal SM [-]	6	3
Optimal Equivalent Storage Hours [h]	24	13
		CAPEX Breakdown
Pyrolysis Plant CAPEX [M€]	20.07	21.44
Heliostat Field + Land Cost [M€]	3.42	1.70
Receiver Cost [M€]	2.58	1.48
Tower Cost [M€]	1.62	0.87
Thermal Energy Storage [M€]	1.03	0.72
Bauxite Particles Cost [M€]	0.49	0.28
Particle Elevator Cost [M€]	0.43	0.16
Solar Plant CAPEX [M€]	9.60	5.23
Total CAPEX [M€]	29.67	26.67
		Annual Performance
Yearly Optical-Thermal Efficiency [-]	0.551	0.549
Fraction of Defocused Energy [-]	0.295	0.071
Pyrolysis Plant Equivalent Hours [h]	7053	8760
Pyrolysis Plant Efficiency [-]	0.786	0.786
Carbon Efficiency [-]	0.908	0.844
ETO [kg <sub>CO2</sub> /GJ <sub>OIL</sub> ]	13.09	21.92
ETO <sub>NET</sub> [kgco2/GJoIL]	-27.05	-19.45
MFSP [€/GJ <sub>OIL</sub> ]	25.71	21.36

#### 4. Conclusion

This study performed the preliminary design and the techno-economic analysis of a 10  $MW_{TH}$  fast pyrolysis plant integrated with a solar rotary kiln particle receiver, obtaining the following results:

- Solar-based pyrolysis can achieve over 90% of carbon efficiency, resulting from about 70% of the inlet biogenic carbon retained in the bio-oil and about 20% of the carbon in the bio-char. Thanks to the carbon stored in biochar, the solar-only mode and the hybrid mode achieve net negative emissions of -27.05 and -19.45 kg<sub>CO2</sub>/GJ<sub>OIL</sub>.
- The constraints on the kiln "rolling mode" flow regime, described by the Froude number limit range, pose a challenge in obtaining good solar field optical efficiencies due to the limited feasible tilt angles, which from the analysis should range between 0.5-2°, and generates challenging solar fluxes on the kiln aperture, whose diameter is constrained to the Froude number. Possible paths to overcome this limit might be to introduce spiral lifters to increase the PHC residence time [28]; to increase the PHC mass flowrate at constant thermal power, thus reducing the ΔT; to consider the adoption of PHCs with low bulk density and heat capacity; or to consider two kilns in parallel halving the mass flowrate.
- Though operating the plant in solar-only mode brings better environmental indexes (i.e ETO: 13.09 vs 21.92 kg<sub>CO2</sub>/GJ<sub>OIL</sub>) thanks to the avoidance of biochar combustion, the lower pyrolysis plant equivalent hours (i.e 7053 vs 8760 h) are a huge drawback due to the high capital investment, thus increasing the payback time and reducing the NPV, favouring the economics of the hybrid mode which has the lowest MFSP (i.e 25.71 vs 21.36 €/GJ<sub>OIL</sub>).

### Data availability statement

Data will be made available on request.

#### **Author contributions**

**Muhammad Ahsan Amjed & Marco Colombi**: Methodology, Investigation, Formal analysis, Software, Visualization, Writing – original draft. **Juan Pablo Rincon Duarte & Clarisse Lorreyte & Gkiokchan Moumin:** Methodology, Investigation, Supervision, Validation. **Matteo C. Romano & Marco Binotti**: Conceptualization, Methodology, Formal analysis, Software, Supervision, Validation, Writing – original draft & review & editing.

# **Competing interests**

The authors declare that they have no competing interests.

# Acknowledgement

This study is funded by the European Union under PYSOLO project (Grant Agreement n. 101118270). Views and opinions expressed are however those of the author(s) only and do not necessarily reflect those of the European Union or CINEA. Neither the European Union nor the granting authority can be held responsible for them.

#### References

[1] Renewable Energy Directive (EU) 2023/2413 of the European Parliament and of the Council of 20 November 2023 on the promotion of the use of energy from renewable sources. ELI: <a href="https://eur-lex.europa.eu/eli/dir/2023/2413/oj">https://eur-lex.europa.eu/eli/dir/2023/2413/oj</a>.

- [2] R. Adib, "Renewables 2023 global status report collection, Renewables in Energy Supply," 2023.
- [3] A. M. Elgarahy, A. Hammad, D. M. El-Sherif, M. Abouzid, M. S. Gaballah, and K. Z. Elwakeel, "Thermochemical conversion strategies of biomass to biofuels, techno-economic and bibliometric analysis: A conceptual review," *J. Environ. Chem. Eng.*, vol. 9, pp. 2213–3437, 2021, doi: 10.1016/j.jece.2021.106503.
- [4] Venderbosch, R. and Prins, W. (2010), Fast pyrolysis technology development. Biofuels, Bioprod. Bioref., 4: 178-208. <a href="https://doi.org/10.1002/bbb.205">https://doi.org/10.1002/bbb.205</a>
- [5] CiP Foundation, "How to establish a market for CCS with biochar in Denmark", 2024,
- [6] V. Chintala, Production, upgradation and utilization of solar assisted pyrolysis fuels from biomass A technical review, Renewable Sustainable Energy Rev., 2018, 90, 120–130, DOI: 10.1016/j.rser.2018.03.066.
- [7] S. Jones, et al., Process Design and Economics for the Conversion of Lignocellulosic Biomass to Hydrocarbon Fuels: Fast Pyrolysis and Hydrotreating Bio-Oil Pathway, 2013.
- [8] M. Rahman, A. Parvej, M. Aziz, "Concentrating technologies with reactor integration and effect of process variables on solar assisted pyrolysis: A critical review", Thermal Science and Engineering Progress, Volume 25, 2021, <a href="https://doi.org/10.1016/j.tsep.2021.100957">https://doi.org/10.1016/j.tsep.2021.100957</a>.
- [9] H. Weldekidan, V. Strezov, G. Town, "Review of solar energy for biofuel extraction", Renewable and Sustainable Energy Reviews, Volume 88, 2018, Pages 184-192, https://doi.org/10.1016/j.rser.2018.02.027.
- [10] PYSOLO Concentrated solar power for biomass pyrolysis. <a href="https://pysolo.eu/">https://pysolo.eu/</a> (29/8/24).
- [11] M.A. Amjed, F. Sobic, M.C. Romano, T. Faravelli, M. Binotti, "Techno-economic analysis of a solar-driven biomass pyrolysis plant for bio-oil and biochar production", 2024, Sustainable Energy & Fuels, The Royal Society of Chemistry, <a href="http://dx.doi.org/10.1039/D4SE00450G">http://dx.doi.org/10.1039/D4SE00450G</a>.
- [12] Aspentech, <a href="https://www.aspentech.com/en/products/engineering/aspen-plus">https://www.aspentech.com/en/products/engineering/aspen-plus</a>, accessed 29/08/24.
- [13] A.Gallo et al., "Considerations for using a rotary kiln for high temperature industrial processes with and without thermal storage", International Solar Energy Society conference proceedings, 2016.
- [14] E.Alonso, A.Gallo, M.I.Roldán, C.A.Pérez-Rábago, E.Fuentealba, "Use of rotary kilns for solar thermal applications: Review of developed studies and analysis of their potential", Solar Energy, Volume 144, 2017, Pages 90-104, https://doi.org/10.1016/j.solener.2017.01.004.
- [15] B.Bisulandu, F.Huchet, "Rotary kiln process: An overview of physical mechanisms, models and applications", Applied Thermal Engineering, Volume 221, 2023, https://doi.org/10.1016/j.applthermaleng.2022.119637.
- [16] C. R. Jones, A. Corona, C. Amador & P. J. Fryer (2021): Dynamics of fabric and dryer sheet motion in domestic clothes dryers, Drying Technology, DOI: 10.1080/07373937.2021.1918706.
- [17] A.Boateng, "Rotary Kilns Transport Phenomena and Transport Process", 2008, ISBN: 978-0-7506-7877-3.
- [18] C.C. Lee, S. Lin (Eds.), Handbook of Environmental Engineering Calculations, McGraw-Hill, New York, 2000.
- [19] M. J. Wagner and T. Wendelin, "SolarPILOT: A power tower solar field layout and characterization tool," *Sol. Energy*, vol. 171, 2018, doi: <a href="https://doi.org/10.1016/j.solener.2018.06.063">10.1016/j.solener.2018.06.063</a>.
- [20] T.Wendelin, A.Dobos, A.Lewandowski, "SolTrace: A Ray-Tracing Code for Complex Solar Optical Systems", 2013, NREL Technical Report.
- [21] C. Frantz, R. Buck, and L. Amsbeck, "Design and Cost Study of Improved Scaled-Up Centrifugal Particle Receiver Based on Simulation," *J. Energy Resour. Technol. Trans. ASME*, vol. 144, no. 9, 2022, doi: 10.1115/1.4053784.
- [22] R. Buck and S. Giuliano, "Impact of CSP design parameters on sCO2-based solar tower plants," 2nd Eur. Supercrit. CO2 Conf., 2018.
- [23] R.Buck, S.Giuliano, "Solar tower system temperature range optimization for reduced LCOE", AIP Conf. Proc. 2126, 030010 (2019), https://doi.org/10.1063/1.5117522.

- [24] Reiner Buck, Jeremy Sment, "Techno-economic analysis of multi-tower solar particle power plants", Solar Energy, Volume 254, 2023, Pages 112-122, <a href="https://doi.org/10.1016/j.solener.2023.02.045">https://doi.org/10.1016/j.solener.2023.02.045</a>.
- [25] EIA, Monthly Densified Biomass Fuel Report, accessed: 8/9/24, <a href="https://www.eia.gov/biofuels/biomass/#table\_data">https://www.eia.gov/biofuels/biomass/#table\_data</a>.
- [26] Q.Kang et al., Particles in a circulation loop for solar energy capture and storage, 2019 Particuology, <a href="https://doi.org/10.1016/j.partic.2018.01.009">https://doi.org/10.1016/j.partic.2018.01.009</a>.
- [27] L. F. González-Portillo, K. Albrecht, and C. K. Ho, "Techno-economic optimization of CSP plants with free-falling particle receivers," Entropy, vol. 23, no. 1, 2021, doi: 10.3390/e23010076.
- [28] G.Moumin, S.Tescari, C.Sattler,"Impact of bed motion on the wall-to-bed heat transfer for powders in a rotary kiln and effect of built-ins", International Journal of Heat and Mass Transfer, Volume 177, 2021, https://doi.org/10.1016/j.ijheatmasstransfer.2021.121473.